Available online at www.sciencedirect.com
SCIENCE DIRECT
Journal of Power Sources 153 (2006) 300–311
JOURNAL OF POWER SOURCES
www.elsevier.com/locate/jpowsour

Surface reactivity of graphite materials and their surface passivation during the first electrochemical lithium insertion

Michael E. Spahr[a,*], Hilmi Buqa[b], Andreas Würsig[b], Dietrich Goers[b], Laurence Hardwick[b], Petr Novák[b], Frank Krumeich[c], Joseph Dentzer[d], Cathie Vix-Guterl[d]

[a] *TIMCAL Ltd., CH-6743 Bodio, Switzerland*
[b] *Electrochemistry Laboratory, Paul Scherrer Institut, CH-5232 Villigen PSI, Switzerland*
[c] *Swiss Federal Institute of Technology (ETH Zürich), Laboratory of Inorganic Chemistry, CH-8093 Zurich, Switzerland*
[d] *Institut de Chimie des Surfaces et Interfaces, CNRS UPR 9069, F-68057 Mulhouse Cedex, France*

Available online 28 June 2005

Abstract

The surface passivation of TIMREX® SLX50 graphite powder was studied as received and after heat treatment at 2500 °C in an inert gas atmosphere by differential electrochemical mass spectrometry in electrochemical lithium half-cells. 1 M $LiPF_6$ in ethylene carbonate and either a dimethyl carbonate, propylene carbonate or 1-fluoro ethylene carbonate co-solvent was used as electrolyte systems in these half-cells. The SEI-film formation properties of both graphite materials were correlated with their active surface area (ASA), being responsible for the interactions between the carbon and the electrolyte system. The active surface area was determined from the amount of CO and CO_2 gas desorbed at temperatures up to 950 °C from the graphite material surface after chemisorption of oxygen at 300 °C. The structural ordering at the graphite surface increased significantly during the heat treatment of the SLX50 graphite material as indicated by the significant decrease of the ASA value. The increased surface crystallinity was confirmed by krypton gas adsorption, Raman spectroscopy as well as temperature-programmed desorption. This increased structural ordering seemed to be the parameter being responsible for a hindered passivation of the heat-treated SLX50 causing partial exfoliation of the graphite structure during the first electrochemical lithium insertion in the ethylene carbonate/dimethyl carbonate electrolyte. In the case of the ethylene carbonate/1-fluoro ethylene carbonate electrolyte system, primarily the fluoro compound is responsible for the graphite passivation. In this electrolyte system, pristine SLX50 and the less reactive, heat-treated SLX50 graphite showed significantly different SEI-film formation mechanisms. In contrast, no difference in the passivation mechanism could be identified for different graphite surfaces in the ethylene carbonate electrolyte system with propylene carbonate as co-solvent.

Keywords: Lithium-ion batteries; Electrochemical lithium insertion; Graphite negative electrode material; Graphite passivation; Electrochemical graphite exfoliation; Active surface area; Graphite surface reactivity

1. Introduction

During the first electrochemical insertion of lithium ions into carbon negative electrodes of secondary lithium batteries, a passivation layer based on electrolyte decomposition products is formed on the surface of the carbon particles. In the ideal case, this so-called solid electrolyte interphase (SEI) layer suppresses any further electrolyte decomposition and, particularly for graphite negative electrode materials with high crystallinity degree, avoids electrochemical exfoliation of the graphite structure [1–3]. The electrolyte composition is a key factor for the formation of an effective SEI layer and thus for the total cell performance [4–8]. The process of graphite surface passivation and SEI formation is irreversible and therefore causes a charge loss, i.e. decreases the energy density of the electrochemical cell. Additionally, the SEI layer on the graphite particle surface influences the cycling stability, high current rate performance as well as the safety of the complete cell [9,10].

* Corresponding author.
E-mail address: M.Spahr@ch.timcal.com (M.E. Spahr).

0378-7753/$ – see front matter © 2005 Elsevier B.V. All rights reserved.
doi:10.1016/j.jpowsour.2005.05.032

Besides the electrolyte system, the surface properties of the graphite negative electrode material play an important role for the formation of the SEI layer. It could be shown recently, that heat treatment of graphite powder with a high degree of graphitization in an inert gas atmosphere above 1300 °C causes electrochemical exfoliation of the graphite structure in ethylene carbonate based electrolyte systems [11–14], an effect that generally has been discussed for graphite materials only in case of electrolyte systems containing propylene carbonate as electrolyte component [15,16]. It could be shown that the heat treatment of the highly crystalline graphite material led to a kinetically hindered passivation of the graphite surface in the ethylene carbonate-based electrolyte during the first electrochemical reduction [14]. The identification and optimization of surface parameters, which affect the quality of the SEI-layer, is a prerequisite for the development of improved graphite electrode materials for advanced lithium-ion batteries.

To identify key parameters of the graphite surface and to better understand their influence on the SEI formation process, we selected the highly crystalline graphite powder as received as well as its heat-treated derivative representing two extreme cases of different graphite surfaces as model systems. These surfaces have been studied with regard to the passivation process in different carbonate electrolyte systems. The results of these electrochemical studies have been used to find correlations with the surface properties of the two graphite materials since in a carbon–liquid interaction, the surface chemical properties of the carbon play a significant role [15]. The surface properties can be described by two different approaches: “a solid state chemistry approach” or an “organic chemistry approach” [16]. This latter approach deals with the nature and the functionality of the oxygen complexes chemisorbed on the edge carbon atoms [17]. The analysis of these surface groups, which are thermally unstable, can be performed by thermal-programmed desorption (TPD) [18]. However, this organic chemistry approach better applies to the description of the surface properties of less ordered carbons (carbon having been prepared at low calcination temperatures). In the frame of this work, the “solid state chemistry” approach seems to be more appropriate. In that approach, the defects in the aromatic basal planes are considered as ‘active sites’ of the carbon surface and the surface carbon solid is characterized in terms of graphitic surface sites [19]. This leads to the concept of the active surface area (ASA) of the graphite material. The procedure to determine values of ASA was developed by Laine et al. [20,21]. In their study, they quantified the role of the carbon active sites in a heterogeneous reaction and found that the carbon ASA was an index for the reactivity of carbon towards oxygen at elevated temperature.

Subsequent works showed that the concept of ASA was equally useful in normalizing the reactivity of different graphite materials towards various species [22–25] and that the concept could be applied to other types of carbon materials (carbon fibres, nanotubes, C/C composites) [26–30]. Therefore, the carbon ASA is an intrinsic graphite property, which is related to the carbon surface reactivity. In this paper, the concept of active sites will be introduced as a parameter to predict the film forming properties of different graphite materials during the first electrochemical reduction of the materials in liquid electrolyte systems. We will try to find correlations between the ASA and the graphite surface reactivity towards carbonate-based liquid electrolyte systems. This should allow to use the ASA method as a quantitative index to compare graphite materials with complementary surface properties with regard to their passivation and SEI-film forming properties in various lithium-ion battery systems and to predict suitable electrolyte systems for every individual graphite surface.

2. Experimental

The synthetic graphite material TIMREX® SLX50 (TIMCAL Ltd., Bodio, Switzerland) was heated at 2500 °C in an inert helium gas atmosphere for 2 days. The sample was cooled down to room temperature and then exposed to air atmosphere.

The crystallinity of the pristine and the heat-treated graphite material was characterized by X-ray diffraction (XRD) measurements using a STOE Stadip diffractometer in Debye-Scherrer geometry and applying monochromatic Cu K(1 radiation (1.5418 Å). The average crystallite size along the crystallographic *c*-axis direction (L_c) and the *a*-axis direction (L_a) were determined from the FWHM of the carbon (0 0 2) and (1 0 0) Bragg diffraction reflexes, respectively, after correction by a factor for the instrumental broadening, using Eq. (1) [31–33].

$$B = \sqrt{B_{\text{exp}}^2 - B_{\text{inst}}^2} \quad (1)$$

In this equation B_{exp} is the FWHM of the graphite Bragg peak. B_{inst} is the instrumental line broadening determined by a silicon standard.

The rhombohedral fraction was derived by the comparison of intensities of the (1 0 1) hexagonal and rhombohedral diffraction peaks [34]. X-ray diffraction (XRD) measurements of the potentiostatically controlled electrodes were carried out using a Bruker AXS D8 Advance diffractometer in Bragg–Brentano geometry working with a secondary monochromator for Cu Kα1 radiation. The particle size distribution of the graphite powders were determined using a MALVERN Mastersizer laser diffractometer.

A confocal Raman microscope (Labram series, Jobin Yvon SA, ex DILOR SA) was used to acquire Raman spectra. The Raman spectra were used to calculate the intensity ratio I_D/I_G of the D-band (1330 cm^{-1}) and G-band (1570 cm^{-1}) as well as the correlation length L_a based on most frequent and average values [35,36]. The original Tuinstra–Koenig relation applied to calculate the L_a value was established for a laser radiation wavelength of 488 nm. The crystallite

size L_a was, therefore, corrected using the correlation factor based on the work of Wang and Dresselhaus [31,37,38]. X-ray photoelectron spectroscopy (XPS) was performed on a VG ESCALAB 220iXL. Details of the XRD, Raman spectroscopy, and XPS measurements were described elsewhere [14].

The nitrogen adsorption properties of the graphite samples were measured using a Micromeritics ASAP 2010 at 77 K and krypton adsorption was performed at the same temperature using a classical volumetric apparatus [39]. For this latter method, thermal transpiration corrections were carried out according to the Takaishi and Sensui formula [40]. Scanning electron microscopy (SEM) pictures were recorded with a JEOL JSM-5600 LV using a heated tungsten anti-cathode.

Electrochemical measurements were performed at 25 °C in a gas-tight, coin-cell-like arrangement [41] using a computer controlled cell capture system (CCCC, Astrol Electronic AG, Oberrohrdorf, Switzerland). Electrodes were prepared by blade-coating the graphite on a copper foil. 10 wt.% polyvinylidene difluoride (SOLEF 1015, Solvay SA) was used as binder. The geometric electrode area was 1.33 cm^2. Metallic lithium (0.75 mm, Alfa Aesar, Johnson Matthey GmbH, Germany) was used as the reference and counter electrode. The electrolyte solvents ethylene carbonate (EC), propylene carbonate (PC), dimethyl carbonate (DMC), as well as the conducting salt $LiPF_6$ applied throughout the measurements had battery quality (Selectipur®, E. Merck, Darmstadt, Germany) and were used as received. The water impurities of the commercial electrolyte systems were controlled by Karl Fischer titration and always were found to be below 50 ppm. Water impurities in 1-fluoro ethylene carbonate (1F-EC) were below 10 ppm. An electrolyte quantity of 0.5 mL was used in every cell. A 1 mm thick soft glass-fibre sheet (Hollingsworth & Vose, Ltd., England) was used as separator. Before the cell assembly, the electrode as well as the glass fibre separator were dried at 120 °C at a reduced argon pressure of 10^{-3} mbar for 12 h and then stored in a dry argon atmosphere.

Unless otherwise stated, galvanostatic measurements were performed at specific currents of 10 mA g^{-1} of carbon to complete the SEI formation in the first Li^+ insertion cycle. After a potential of 5 mV versus Li/Li^+ was reached in the first galvanostatic Li^+ insertion, the discharging was continued potentiostatically until the specific current dropped below 5 mA/g. The electrochemical lithium de-insertion was performed at a constant specific current of 10 mA g^{-1} until a cut-off potential of 1.5 V versus Li/Li^+ was reached and a subsequent potentiostatic stabilization at this potential until the specific current dropped below 5 mA g^{-1}. The same cells were used for the post mortem SEM and XRD studies. The cells were dismantled, the negative electrodes washed thoroughly with dry DMC, and dried in a dry argon atmosphere.

Differential electrochemical mass spectrometry (DEMS) was used to study the processes of electrolyte decomposition and SEI formation, and to follow the formation of ethylene, propylene, and/or carbon dioxide on graphite electrodes during the first electrochemical reduction in different carbonate-based electrolyte solutions. The DEMS set-up has been described elsewhere [42]. The method is based on the non-wettability of a porous membrane that acts as a solvent barrier between the electrochemical cell and the vacuum system of the mass spectrometer. A porous working electrode prepared using a spray technique is deposited onto the membrane. The active mass of the electrodes was about 4 mg cm^{-2}.

Temperature-programmed desorption was performed in a vacuum system equipped with a mass spectrometer at a maximum pressure of 10^{-4} Pa. The graphite sample was deposited in a fused silica tube and heat-treated up to 1000 °C with a linear heating rate of 10 °C min^{-1}. During the experiment, the gas phase was continuously analyzed quantitatively by the mass spectrometer. Before the experiment, the mass spectrometer was calibrated using H_2 ($m/z = 2$), H_2O ($m/z = 10$), CO ($m/z = 28$), N_2 ($m/z = 28$), O_2($m/z = 32$), and CO_2 ($m/z = 44$) gases. The quantitative determination of functional groups was based on H_2, H_2O, CO, and CO_2, as the amount of O_2 and N_2 was found to be negligible. The total gas pressure evolved during the heat treatment was measured as a function of the temperature using a Bayard-Alpert gauge. The total gas pressure was compared to the pressure calculated from the sum of the partial pressure of the gas species deduced from the quantitative analysis of the gas stream. The discrepancy between the calculated pressure and the measured pressure was attributed to the presence of hydrocarbons C_xH_y with $x > 2$ in the gas phase.

The active surface area was determined by outgassing the sample in the same experimental set-up at 950 °C under vacuum (10^{-4} Pa). An initial oxygen pressure of 66.5 Pa was introduced in the reactor at 300 °C causing a chemisorption of O_2 on the graphite surface. The O_2 chemisorption process over a period of 15 h at 300 °C led to the formation of surface oxide complexes at a specific part of the graphite surface area, i.e. the graphite active sites area. The amount of oxygen complexes formed was determined by measuring the amount of CO and CO_2 desorbed from the graphite surface at temperatures higher than the complex formation temperature by performing a TPD step between 300 and 950 °C. The amount of CO and CO_2 that desorbed was measured with the mass spectrometer. By determining the number of moles of each gas desorbed and taking the area of an edge carbon site that chemisorbed an oxygen atom as 0.0083 nm^2, the surface area occupied by chemisorbed oxygen can be calculated [20,21].

3. Results and discussion

3.1. Electrochemical characterization

TIMREX® SLX50 is a typical representative of the family of highly crystalline graphite negative electrode materials which electrochemically insert lithium up to a chemical composition of LiC_6, being equivalent to a theoretical

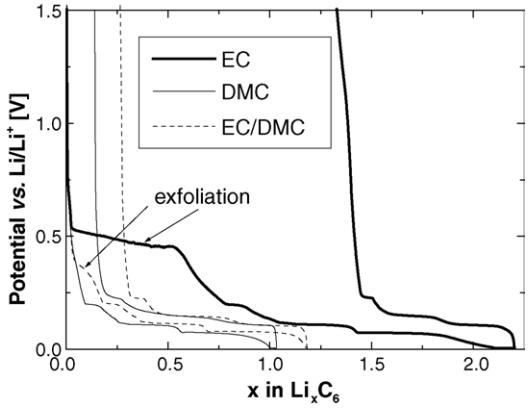

Fig. 1. First electrochemical lithium insertion/de-insertion into TIMREX® SLX50 (HT) using either ethylene carbonate, dimethyl carbonate or ethylene carbonate/dimethyl carbonate 1:1 (w/w) as electrolyte solvents.

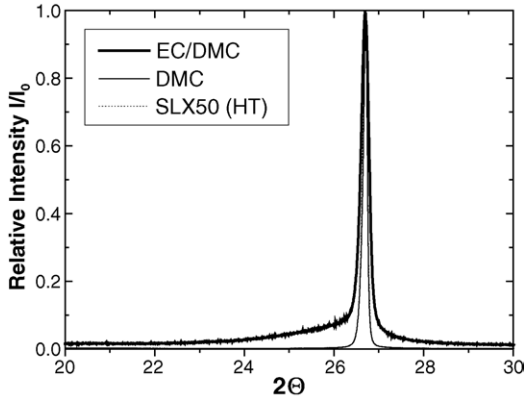

Fig. 2. (0 0 2) X-ray diffraction peak of heat-treated TIMREX® SLX50 graphite electrodes taken from half-cells, which were discharged galvanostatically at 10 mA g^{-1} to the cut-off potentials 0.3 V vs. Li/Li^+, respectively, and then potentiostatically stabilized at these potentials for 2 days using 1 M $LiPF_6$ in either ethylene carbonate or dimethyl carbonate as electrolyte. The X-ray diffraction peak of the heat-treated SLX50 powder shown for comparison is hardly distinguishable from the DMC case.

reversible capacity of 372 mAh g^{-1} of carbon. Typically, a reversible capacity of about 365 mAh g^{-1} and a coulombic efficiency of 93% can be observed in the first galvanostatic charge/discharge cycle for the SLX50 negative electrode material at a specific current of 10 mA g^{-1} using PVDF as binder and $LiPF_6$ in EC/DMC 1:1 (w/w) as electrolyte [12]. Heat treatment of the SLX50 graphite material resulted in a graphite material SLX50 (HT) showing the same particle size distribution as the starting graphite: Laser diffraction measurements indicated an average particle size of 22 μm and a $d_{90\%}$ value of 56 μm for both the heat-treated SLX50 and the SLX50 as received.

In contrast to SLX50, SLX50 (HT) shows an additional irreversible electrochemical process during the first electrochemical reduction, indicated in the galvanostatic potential curve by the potential plateau at about 0.45 V versus Li/Li^+ (Fig. 1). This irreversible process significantly increases the loss of specific charge during the first electrochemical lithium insertion. Using pure ethylene carbonate instead of the EC/DMC mixture as electrolyte solvent, this potential plateau increases in size and shifts to more positive potentials of about 0.55 V versus Li/Li^+. Using DMC as single electrolyte solvent, the irreversible process disappears, as shown in Fig. 1. Conclusively, the irreversible electrochemical process apparently only occurs in the presence of ethylene carbonate as electrolyte component.

Post mortem XRD studies of the discharged graphite electrode were performed by especially focusing on the (0 0 2) diffraction peak that corresponds to the X-ray diffraction at the graphite planes. As shown in Fig. 2, the (002) XRD peak of the SLX50 (HT) electrode, which was discharged to 0.3 V versus Li/Li^+ in the mixed EC/DMC (50%:50%, w/w) electrolyte system broadens towards smaller 2Θ angles compared to the SLX50 (HT) starting material. The asymmetric peak broadening indicates a random expansion of the graphite layers and an increase of the interlayer distance. In contrast, the XRD diffraction pattern of the SLX50 (HT) electrode material, which was discharged in the pure DMC electrolyte does not change compared to the diffraction pattern of the SLX50 (HT) starting material. The SEM picture in Fig. 3 taken from the discharged graphite electrode of the dismantled half-cell containing the EC/DMC electrolytes indicates exfoliation of a fraction of the graphite particles in the electrode. Gaps and holes observed at the graphite layer edges (prismatic surfaces) of the defective graphite particles indicate only a partial exfoliation, i.e. the exfoliation of only some single crystals in the graphite particle. The electrochemical exfoliation process observed increases the wetted electrode surface area thus leading to the increase of irreversible capacity observed for the SLX50 (HT) in comparison to the untreated SLX50. Besides the partial exfoliation of the graphite particle, a relatively thick layer presumably of electrolyte decomposition products could be detected at the graphite particle surface indicating a strong electrolyte decomposition process occurred before the passivation of the graphite surface could be achieved.

3.2. Graphite material bulk and surface analyses

To understand the modifications created in the graphite material during the heat treatment, the crystal structure of the untreated and heat-treated SLX50 was characterized by XRD. As summarized in Table 1, the increased L_c and L_a values calculated from the XRD patterns indicate significantly increased single crystals in the graphite particles of the

Table 1
Structural bulk parameters of TIMREX® SLX50 before and after heat treatment at 2500 °C obtained from X-ray diffraction measurements

	SLX50	SX50 HT
L_c (002) (nm)	35 (±5)	72 (±11)
L_a (100) (nm)	64 (±10)	77 (±12)
Fraction of rhombohedral stacking defects (%)	23 (±2)	0

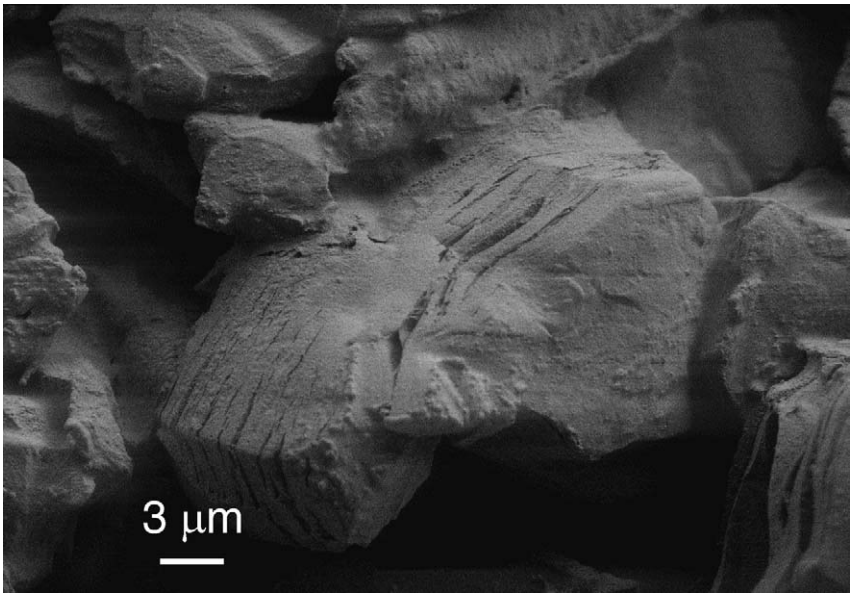

Fig. 3. SEM picture of a heat-treated SLX50 graphite negative electrode taken from a half-cell, which was discharged galvanostatically at 10 mA g^{-1}–0.3 V vs. Li/Li^+ and stabilized potentiostatically at this potential for 2 days using 1 M $LiPF_6$ in EC:DMC 1:1 (w/w) as electrolyte.

heat-treated graphite material. In addition, the rhombohedral stacking faults in the graphite structure completely vanished during the heat-treatment. Due to the smaller penetration depth of the Raman laser beam (some micrometers) compared to the X-ray beam, Raman spectroscopy was used to characterize the crystallinity in the surface-near regions of the graphite particles. The correlation length L_a, calculated from the intensity ratio of the D-band and G-band of the Raman spectra, drastically increases during the heat treatment of the graphite material, as shown in Table 2. This indicates a significantly decreased amount of disordered carbon at the heat-treated surface, i.e. an increased surface crystallinity. The heat treatment has a healing effect on the graphite bulk and surface decreasing the amount of crystal defects as well as the defects at the graphite surface. In addition, the results of the XRD and Raman experiments indicate that the heat treatment stronger affects the crystallinity in the surface-near regions of the graphite particle than in its bulk volume. This result could be confirmed by surface morphology studies using krypton absorption measurements, which are summarized in Table 2. The heat treatment of the SLX50 graphite causes a significant increase of the basal plane surfaces, to the detriment of the prismatic surfaces (edge planes) and low energy defects like dislocation lines at the graphite surface. The significant increase of the structural ordering also is confirmed by the ASA measurements as explained further. The concentrations of surface oxides linked to the superficial defects were studied by X-ray photoelectron spectroscopy (XPS). In comparison to the untreated graphite surface, the results of the XPS measurements indicates a slight decrease of the oxygen concentration at the heat treated graphite surface and therefore are in line with the other surface characterization measurements.

Table 2
The results of Raman spectroscopy, krypton gas adsorption, and X-ray photo electron spectroscopy measurements, describing the surface properties of TIMREX® SLX50 before and after heat treatment at 2500 °C

	SLX50	SLX50 HT
Raman spectroscopy		
L_a (nm)	25	140
Krypton gas adsorption		
Total surface area ($m^2\ g^{-1}$)	4.0	2.8
Fraction of basal plane surfaces (%)	42	67
Fraction of prismatic surfaces (polar edges) (%)	25	9
Fraction of low energy defects (%)	33	24
X-ray photo electron spectroscopy		
O (1s) (at.%)	1.2	0.6
C (1s) (at.%)	98.3	99.0

Temperature-programmed desorption is a powerful tool to characterize the amount and nature of the surface groups at the graphite surface. The amount and nature of gaseous species desorbed from the graphite surface between 100 and 1000 °C at reduced pressure of 10^{-4} Pa is continuously analyzed by mass spectroscopy. In the case of graphite materials like the pristine SLX50, besides some hydrocarbons, usually only H_2, H_2O, CO, and CO_2 can be detected (Fig. 4). Besides the physiosorbed H_2O molecules at the graphite surface, the desorption of water molecules in combination with desorbed CO_2 is assigned to the decomposition of carboxylic surface groups, typically occurring between 250 and 600 °C. The desorption of CO from the graphite surface with a maximum between 600 and 800 °C describes the thermal decomposition of carbonyl and phenol surface groups. The desorption of hydrogen above 850 °C relates to structural reorganisation of superficial less organised carbon and could indicate the

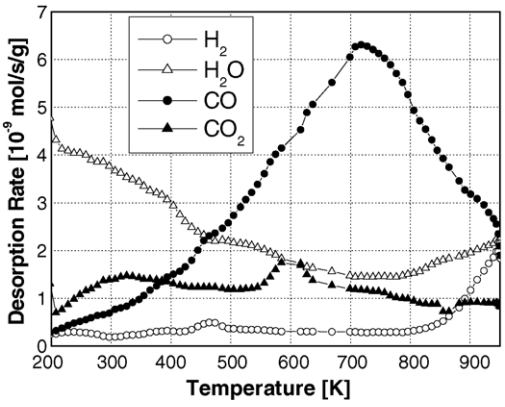

Fig. 4. H_2, H_2O, CO, and CO_2 gas desorbed from the TIMREX® SLX50 surface up to 950 °C in temperature-programmed thermodesorption experiments.

initial crystallization process at the surface of the SLX50 graphite material. As illustrated in Fig. 5, in comparison to the untreated SLX50, the nature of the thermal stability of the formed oxygen complexes are different. The functional groups being present at the SLX50 (HT) surface are thermally more stable. It also appears in this figure that the desorption rates of CO and CO_2 gas are much lower for SLX50 (HT). Consequently, the total amount of CO and CO_2 desorbed from the SLX50 (HT) surface drops significantly, as summarized in Table 3.

3.3. Study of the electrochemical graphite passivation process

To find an explanation for the electrochemical exfoliation which occurs in EC containing electrolytes for the heat-treated SLX50 in contrast to the untreated SLX50, differential electrochemical mass spectrometry was performed in an electrochemical half-cell connected to a mass spectrometer. The evolution of volatile species was monitored as a function of the graphite potential for the first two consecutive electrochemical insertion/de-insertion cycles of lithium ions into

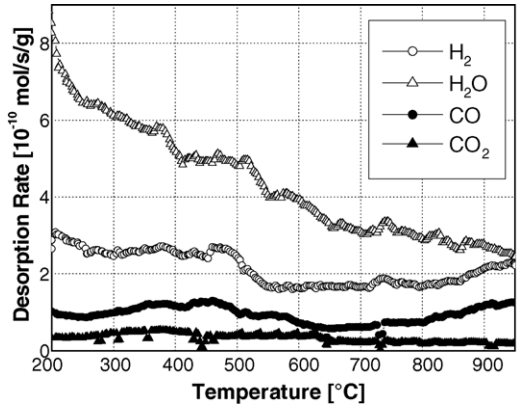

Fig. 5. H_2, H_2O, CO, and CO_2 gas desorbed from the surface of SLX50 (HT) up to 950 °C in temperature-programmed thermodesorption experiments.

Table 3
Amount of desorbed H_2, H_2O, CO, and CO_2 gas obtained in temperature-programmed desorption measurements of TIMREX® SLX50 and SLX50 (HT) up to 950 °C as well as the active site surface area, the active site surface area normalized to the total specific BET surface area (d_{ASA}), and the amount ratio of CO and CO_2 desorbed up to 950 °C, which was determined for TIMREX® SLX50 and SLX50 (HT) in the same experimental set-up after oxygen chemisorption at 300 °C

TPD results	SLX50	SLX50 (HT)
TSA ($m^2\,g^{-1}$)	4.0	2.6
H_2 ($\mu mol\,m^{-2}$)	0.55	0.4
H_2O ($\mu mol\,m^{-2}$)	3.25	5
CO ($\mu mol\,m^{-2}$)	3.75	1
CO_2 ($\mu mol\,m^{-2}$)	1.48	0.33
ASA ($m^2\,g^{-1}$)	0.3	0.008
d_{ASA} = ASA/TSA	0.08	0.003

both SLX50 and SLX50 (HT) using a mixed EC/DMC 1:1 (w/w) electrolyte system. Due to the high electrolyte viscosity leading to problems in the detection of volatile species formed at the negative electrode, the measurement was not possible in the pure EC electrolyte. In the case of untreated SLX50, a mass signal of $m/z = 27$ corresponding to ethylene gas could be detected by the mass spectrometer starting at 1.1 V versus Li/Li^+ as shown in Fig. 6. Ethylene is considered as typical reductive decomposition product of the ethylene carbonate electrolyte. For the example of the electrochemical decomposition of DMC on graphite surfaces, no ethylene gas but H_2 and CO gas could be detected starting at electrochemical potentials above 1.5 V versus Li/Li^+. Thus, the ethylene formation observed in the DEMS experiment can be assigned to the decomposition of the ethylene carbonate electrolyte component at the graphite electrode surface. The ethylene signal has a maximum at 0.55 V versus Li/Li^+ and almost disappears at potentials below 0.2 V versus Li/Li^+ indicating the completion of the graphite surface passivation process. Apparently, the DMC component does not achieve complete passivation of the graphite surface during its decomposition at more positive potentials. In the mixed EC/DMC electrolyte system, also the EC component participates at the graphite surface passivation process and finally achieves the formation of an effective SEI-film which suppresses further electrolyte decomposition. The formation of ethylene is accompanied by the formation of hydrogen observed at potentials below 0.45 V versus Li/Li^+. The delay of the hydrogen formation compared to the ethylene formation could indicate a change of the ethylene carbonate decomposition mechanism at less positive potentials or another decomposition process of the DMC component. In the second cycle, almost no gas evolution can be observed indicating an efficient graphite passivation for SLX50 during the first lithium insertion process in the EC/DMC electrolyte system.

In contrast to the untreated SLX50, the initial ethylene formation is shifted below 0.55 V versus Li/Li^+ for SLX50 (HT). Thus, the graphite exfoliation process sets in before graphite passivation by the formation of an efficient SEI-film is accomplished at the graphite surface. The maximum

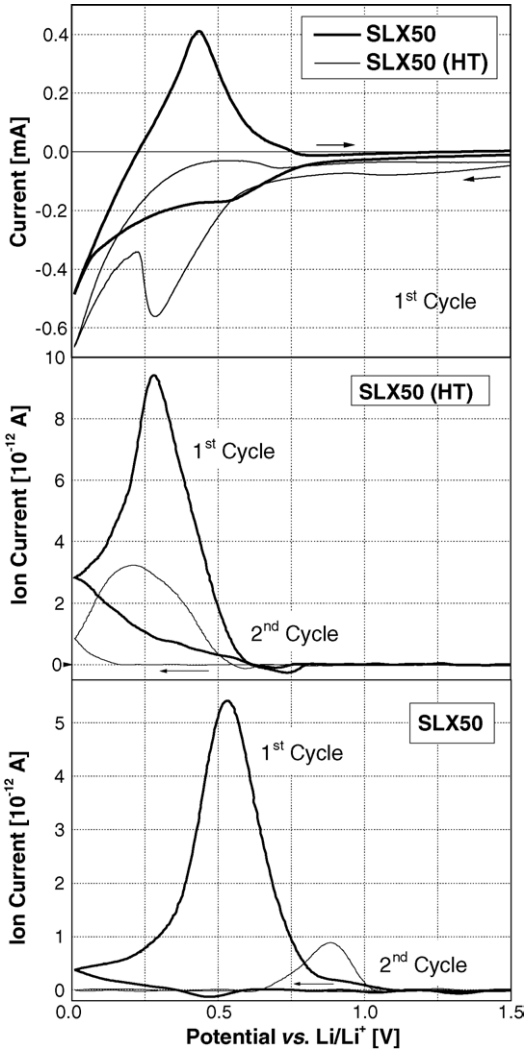

Fig. 6. Differential electrochemical mass spectrometry (DEMS) measurements in half-cells containing TIMREX® SLX50 and SLX50 (HT) as electrodes and 1 M $LiPF_6$ in EC:DMC 1:1 (w/w) as electrolyte. The mass signal $m/z = 27$ corresponding to the ethylene formation was monitored as a function of the potential applied to the graphite electrode at a scan rate of 0.4 mV s^{-1}. The cyclic voltammogram of the cells was simultaneously measured.

amount of ethylene is formed at about 0.3 V versus Li/Li^+ but does not stop with the cell potential decreasing further. Due to the formation of new surfaces during the exfoliation process, electrolyte decomposition proceeds at the potential range in which the insertion of lithium ions into the graphite material takes place and continues even in the following de-insertion process. Also in the second charge/discharge cycle, a relatively high level of ethylene gas formation can be observed indicating that no efficient SEI layer formation is achieved on the heat-treated graphite surface.

The passivation film formation is hindered at the heat-treated graphite surface that apparently shows a decreased surface reactivity in comparison to the pristine graphite surface. The reactivity of the graphite surface towards the electrolyte can be enhanced by increasing the temperature during

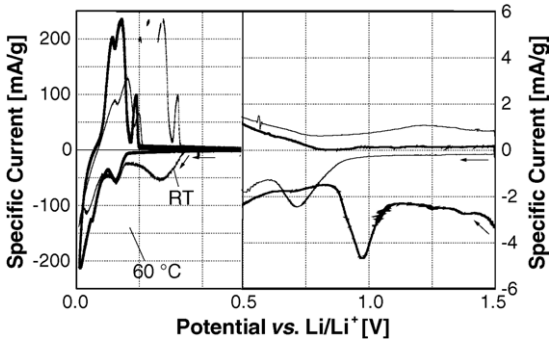

Fig. 7. Cyclic voltammograms (first cycle) of SLX50 (HT) performed at room temperature (thin line) and 60 °C (bold line), respectively, using 1 M $LiPF_6$ in EC:DMC 1:1 (w/w) as electrolyte system at a scan rate of 10 μV s^{-1}.

the graphite passivation process as shown in Fig. 7. The cyclic voltammogram shows the first electrochemical insertion of lithium ions in SLX50 (HT) at room temperature using the mixed EC/DMC electrolyte system. The graphite exfoliation process appears as irreversible cathodic peak at about 0.35 V versus Li/Li^+. This irreversible peak completely disappears at a film formation temperature of 60 °C. An expansion of the specific current axis reveals at 60 °C a cathodic current positive to 1.5 V versus Li/Li^+, which indicates a shift of the initial film formation to more positive potentials. This shift could be confirmed by DEMS measurements shown in Fig. 8. The initial ethylene formation shifts from 0.55 V versus Li/Li^+ in the case of a film formation at room temperature to about 0.85 V versus. Li/Li^+ at a film formation temperature of 60 °C. At elevated temperature also the signal intensity increased caused either by a higher electrolyte decomposition rate or by a decreased solubility of the ethylene gas in the electrolyte system. It seems obvious that the hindrance of the graphite passivation is a kinetic effect and, besides the electrolyte film forming properties, is directly related to the

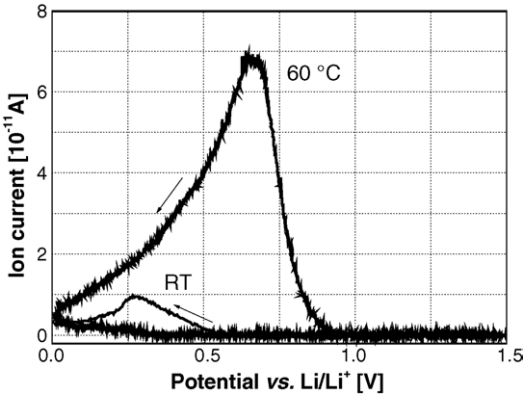

Fig. 8. Differential electrochemical mass spectrometry (DEMS) measurements at room temperature and 60 °C in half-cells containing SLX50 (HT) as graphite electrode and 1 M $LiPF_6$ in EC:DMC 1:1 (w/w) as electrolyte. The mass signal $m/z = 27$ corresponding to the ethylene formation was monitored as a function of the potential applied to the electrochemical cell at a scan rate of 0.4 mV s^{-1}.

reactivity of the individual graphite surface. To be able to compare the reactivity of different graphite surfaces towards a given electrolyte system, the active surface area of SLX50 and SLX50 (HT) was measured and correlated with their passivation properties.

3.4. Active surface area of graphite

The concept of the active surface area is based on the fact, that during chemisorption of oxygen at outgassed carbon surfaces at 300 °C and an oxygen partial pressure of 50–100 Pa, surface oxygen complexes are formed on a specific part of the graphite surface which are called active surface area. The ASA is composed of active sites that exist on the carbon surface where the carbon atom valency is not satisfied. On a "clean" graphite surface, these active sites would be located on the edges of the exposed graphene layer planes (prismatic surfaces) as well as at points of imperfection in the graphite structure including vacancies, dislocations and steps in the outer basal plane surfaces [22]. They can be attributed to structural features, heteroatoms (O, S, N), and mineral matter. The amount of oxygen complexes formed on these active sites after oxygen chemisorption at 300 °C is determined by measuring the amount of CO and CO_2 evolved in a subsequent thermodesorption experiment from temperatures above the chemisorption temperature up to 950 °C since it was shown that CO and CO_2 are primary species of the oxide complex decomposition [20–22]. As shown in Fig. 9, the amount of CO and CO_2 which was desorbed from the surface of the SLX50 (HT) after the chemisorption process is significantly smaller than for the SLX50. This result is reflected in the values for ASA and d_{ASA} which corresponds to the amount of active sites and the density of active sites (d_{ASA}), respectively (Table 3). d_{ASA} is defined as the fraction of ASA related to the total graphite surface area and therefore is calculated by normalizing the ASA to the total surface area (TSA) of the graphite material, determined by the BET method. For the heat-treated SLX50, ASA and d_{ASA} are more than one order of magnitude smaller than for the untreated SLX50. This result confirms that the heat treatment of the SLX50 leads to a significant increase of the structural ordering of the carbon. The d_{ASA} value of the SLX50 sample indicates that its surface has a larger amount of active sites and consequently has a more heterogeneous surface than the heat-treated SLX50 material. For SLX50 (HT), the value of ASA being less than 0.3% of the TSA reflects a very homogeneous surface which essentially is composed of basal planes. During the annealing process, superficial defects apparently were changed to basal planes. The low ASA value of SLX50 (HT) allows to predict, compared to the pristine SLX50 graphite material, a decreased reactivity of the heat-treated graphite surface towards the electrolyte system. The decreased reactivity of SLX50 (HT) causes, during its first electrochemical reduction, the initial decomposition of the electrolyte system at less positive potentials than SLX50 and correlates with the observed passivation and film forming properties of SLX50 and SLX50 (HT) described above. The results of the chemisorption experiments are consistent with the results found by Raman spectroscopy. This is not surprising since ASA can be correlated to the L_a (in-plane correlation length) parameter determined by Raman spectroscopy as recently explained [30].

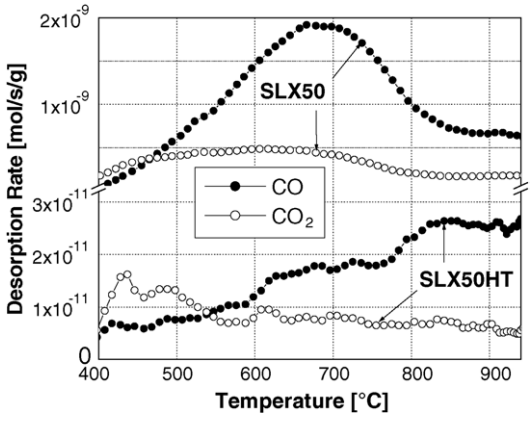

Fig. 9. The desorption of CO and CO_2 gas as a function of the temperature measured in temperature-programmed thermodesorption experiments of TIMREX® SLX50 and SLX50 (HT) after chemisorption of oxygen at 300 °C and an oxygen partial pressure of 50–100 Pa.

3.5. Effect of other cyclic carbonate electrolyte components

In the following, the differences in reactivity of the pristine and heat-treated graphite surface is studied for ethylene carbonate based electrolyte systems containing, instead of the acyclic dimethyl carbonate, either cyclic propylene carbonate or 1-fluoroethylene carbonate as second electrolyte component. Compared to ethylene carbonate, propylene carbonate having an additional methyl group is expected to have a higher electron density in the dioxolane part of the molecule leading to a energetically higher LUMO and thus showing a higher stability towards reductive potentials. The electron-withdrawing effect of the fluorine atom in the 1F-EC molecule is expected to cause a reduction of the electron density in the dioxolane ring leading to a lower LUMO and a higher reactivity towards reductive potentials.

Fig. 10 compares the cyclic voltammograms of the first lithium insertion into untreated and heat-treated SLX50 using 1 M $LiPF_6$ in EC/PC 1:1 (w/w) as electrolyte system. Both cyclic voltammograms show a huge irreversible cathodic peak describing the electrochemical exfoliation of the graphite structure. For both the pristine and the heat-treated SLX50 graphite, the irreversible process starts at about 0.9 V versus Li/Li^+. Compared to the EC/DMC electrolyte, the specific charge related to the reversible lithium insertion process below 0.25 V versus Li/Li^+ is significantly smaller in case of SLX50, for SLX50 (HT) no lithium insertion can be observed at all. An explanation could be that the electrochemical exfoliation process leads to a complete

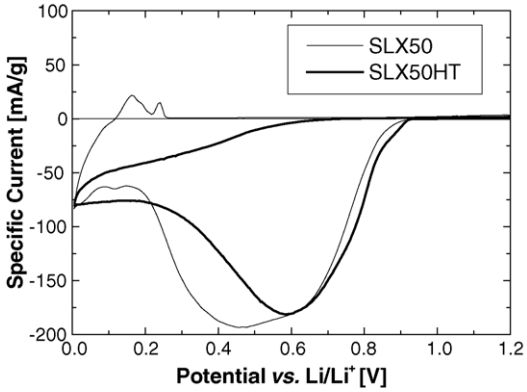

Fig. 10. First cycle cyclic voltammograms of TIMREX® SLX50 and SLX50 (HT) performed at a scan rate of 10 μV s^{-1} using 1 M $LiPF_6$ in EC/PC 1:1 (w/w) as electrolyte.

destruction of the graphite structure. The remaining poorly organized carbon does not allow any lithium insertion.

Post mortem XRD studies of the SLX50 (HT) electrode material after being discharged to 0.3 V versus Li/Li^+ resulted in a diffraction pattern which shows significantly decreased peak intensities and a high background noise as shown in Fig. 11 in comparison to the SLX50 (HT) powder. Compared to the SLX50 (HT) electrode material discharged in the EC/DMC based electrolyte, almost no asymmetric peak broadening is observed for the (0 0 2) diffraction peak showing no significant exfoliation of the graphite structure. The shift of the (0 0 2) peak to higher Bragg angles is presumably due to the increase of the electrode thickness, that is caused by pronounced exfoliation. This can affect the X-ray beam geometry. The diffusion bands centered at 2Θ values of about 22°, 32°, and 37° indicate one or more "amorphous" phases. So far, the nature of these phase(s) could not yet be identified. The significant increase of the background intensity indicates that many of the graphite crystals of the electrode material have been transferred to the amorphous state during the irreversible process of the first electrochemical reduction. It could be possible that the electrochemical exfoliation process occurring in the EC/PC system is drastic and occurs in most of the single crystals of the graphite particles. As consequence, the graphite particles crack and fall apart. Furthermore, the graphite structure is completely destroyed by the exfoliation process.

The mass signals of the DEMS measurement showed no significant difference between SLX50 and SLX50 (HT) in case of the EC/PC electrolyte, as illustrated in Fig. 12, indicating a similar reactivity of the electrolyte system on the

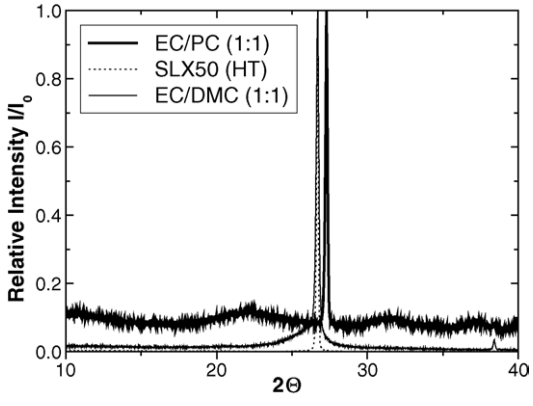

Fig. 11. (002) X-ray diffraction peak of heat-treated TIMREX® SLX50 as well as SLX50 graphite electrodes taken from half-cells, which were discharged galvanostatically at 10 mA g^{-1} to the cut-off potentials 0.3 V vs. Li/Li^+ and subsequently potentiostatically stabilized at this potentials for 2 days using using ethylene carbonate/propylene carbonate 1:1 (w/w) or ethylene carbonate/dimethyl carbonate 1:1 (w/w) as electrolyte solvents.

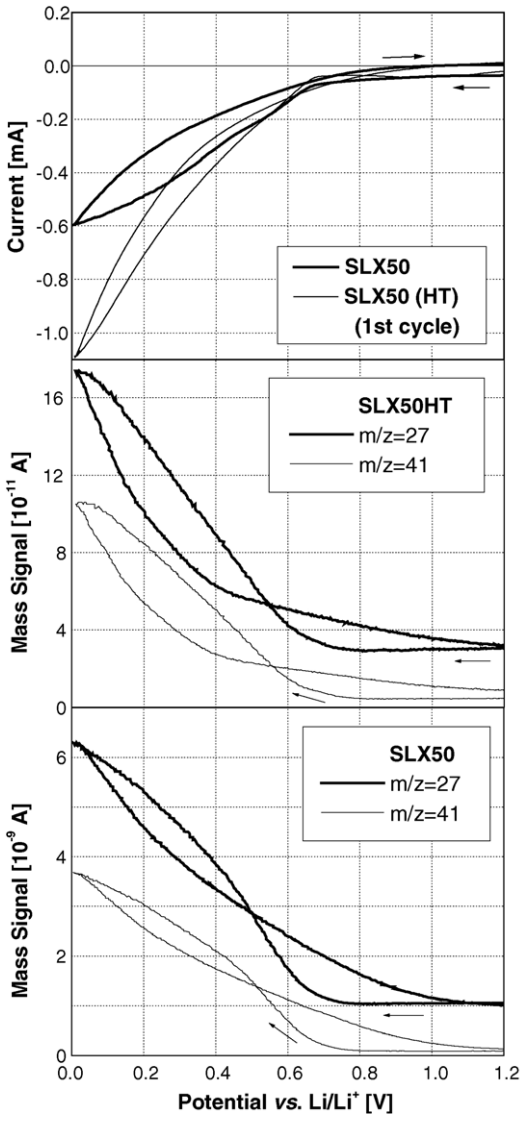

Fig. 12. Differential electrochemical mass spectrometry (DEMS) measurements in half-cells containing TIMREX® SLX50 and SLX50 (HT) as electrodes and 1 M $LiPF_6$ in EC:PC 1:1 (w/w) as electrolyte. The mass signal $m/z = 27$ corresponding to the ethylene formation was monitored along with the mass signal $m/z = 41$ corresponding to the propylene formation, as a function of the potential applied to the electrochemical cell at a scan rate of 0.4 mV s^{-1}. The curves were arbitrarily shifted on the vertical scale. The cyclic voltammogram of the cells was simultaneously measured.

untreated and heat-treated graphite surface. The EC/PC electrolyte system does not distinguish between different graphite surface reactivities. This is in contrast to the EC/DMC electrolyte system and points to a different electrolyte decomposition and film forming mechanism in the PC-containing EC electrolyte system. The initial ethylene and propylene formation could be detected for both surfaces at about 0.75 V versus Li/Li$^+$, which is less positive than the irreversible process observed in the cyclic voltammogram at about 0.9 V versus Li/Li$^+$. Thus, the degradation of the graphite structure is initiated before an effective graphite surface passivation takes place. The gas formation rate increases with decreasing potential. The DEMS experiment at a scan rate of 0.4 mV s^{-1} showed ethylene gas formation also during the charging process of the half cell between 0 and about 1 V versus Li/Li$^+$. The exfoliation of the graphite structure creates new fresh surfaces that decompose electrolyte and form ethylene as one decomposition product. Since the exfoliation process is not accomplished in the discharge process at a scan rate of 0.4 mV s^{-1}, gas formation can be observed in the subsequent charging process of the electrode. The relatively high scan rate of 0.4 mV s^{-1} was chosen in the DEMS experiment to increase the ethylene gas concentration in the mass spectrometer for a sufficient resolution.

Propylene gas formation being the typical decomposition product of the propylene carbonate starts at the same potential as the ethylene gas formation, originated from the decomposition of the ethylene carbonate at the graphite electrode. Due to the high intensity of the mass signal at $m/z = 27$, it can be excluded that the ethylene gas detected in the mass spectrometer is a fragment of the propylene gas. Since a quasi identical behavior of the ethylene and propylene gas formation can be observed, the mixed EC/PC electrolyte system could be considered as a quasi single component electrolyte system. The mixed EC/PC electrolyte shows a lower electrochemical reactivity than the pure EC electrolyte system at the graphite electrode. The film formation in the EC/PC system is hindered on both graphite surfaces and does not depend on the nature of the graphite surface reactivity. EC is able to passivate only relatively reactive graphite surfaces with a high active surface area.

The difference in reactivity between EC and PC is linked to the methyl group of PC which increases the electron density in the five-membered ring of the cyclic carbonate. In the case of a lower electron density in the ring, the stability of the electrolyte towards reductive electrode potentials should decrease. This is confirmed by the good passivating properties of the 1F-EC, shown in Figs. 13 and 14. The cyclic voltammograms does not show any irreversible process corresponding to electrochemical exfoliation. The extension of the specific current axis reveals the significant cathodic current already observed at 1.75 V versus Li/Li$^+$ in the first electrochemical reduction indicating the start of the passivation layer at potentials being significantly more positive than the potential at which the electrochemical exfoliation process is expected. The decomposition of the 1F-EC occurs on graphite surfaces

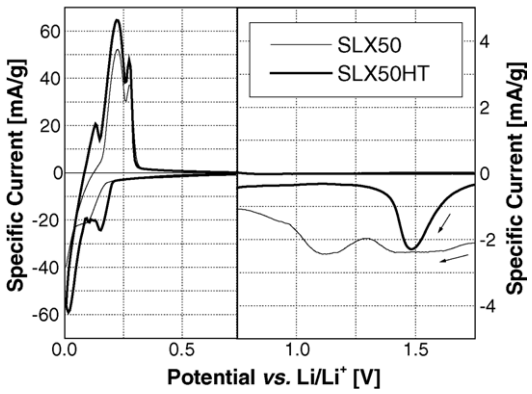

Fig. 13. Cyclic voltammogram (first cycle) of TIMREX® SLX50 and SLX50 (HT) using 1 M $LiPF_6$ in EC:1-fluoroethylene carbonate 1:1 (w/w) as electrolyte system at a scan rate of 10 μV s^{-1}.

independent of their surface reactivity, i.e. even for graphite surfaces with small active surface areas.

DEMS of half-cells containing a SLX50 graphite electrode and an EC/1F-EC (1:1) electrolyte detected no ethylene gas but CO_2 gas formation. It can be concluded that only the 1F-EC component is responsible for the graphite passivation

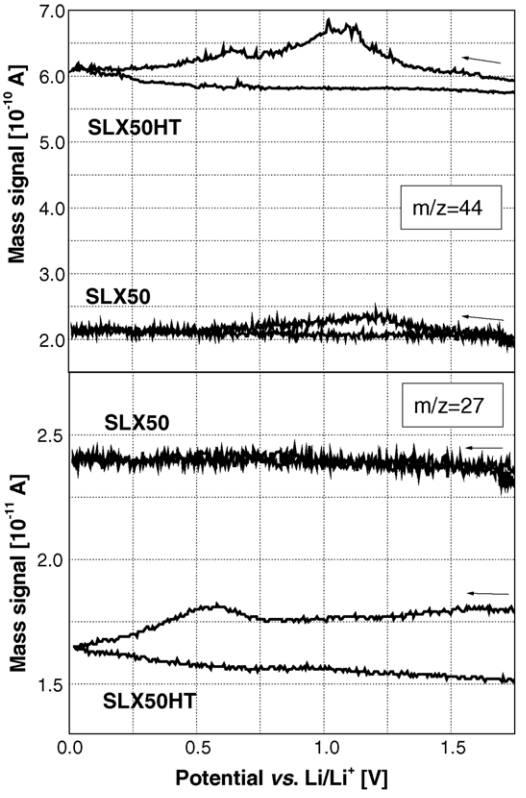

Fig. 14. Differential electrochemical mass spectrometry (DEMS) measurements in half-cells containing TIMREX® SLX50 and SLX50 (HT) as electrodes and 1 M $LiPF_6$ in EC:1-fluoroethylene carbonate 1:1 (w/w) as electrolyte system. The mass signal $m/z = 27$ corresponding to the ethylene formation was monitored along with the mass signal $m/z = 44$ corresponding to the carbon dioxide formation, as a function of the potential applied to the graphite electrode at a scan rate of 0.4 mV s^{-1}.

in the mixed EC/1F-EC electrolyte system. The passivation of the highly crystalline graphite surface in the 1F-EC-based electrolyte follows the same decomposition mechanism as in the 1-chloroethylene carbonate electrolyte system reported elsewhere [43,44]. This difference from the reductive decomposition of EC which results in mainly ethylene and hydrogen formation, besides the non-volatile compounds, which cannot be detected by DEMS. Since 1F-EC already decomposes at potentials above 1.75 V versus Li/Li$^+$, the protective SEI layer is formed at potentials being more positive than the potential at which the EC decomposition would set in.

For the example of heat-treated SLX50 surface, both ethylene and CO_2 gas can be observed in the DEMS measurement. The CO_2 formation starts at about 1.5 V versus Li/Li$^+$ which is similar as in the case of the untreated SLX50. The maximum of the CO_2 formation is observed at 1.1 V versus Li/Li$^+$ and is slightly less positive than in case of the untreated SLX50. A second CO_2 peak is detected starting at 0.75 V versus Li/Li$^+$, which is the same potential at which the ethylene composition can be detected. In the case of heat-treated graphite electrode material with low amount of active surface sites, graphite passivation cannot be accomplished only by the 1F-EC electrolyte component at potentials above 1 V versus Li/Li$^+$. Therefore, the SEI-film formation is completed below 1 V versus Li/Li$^+$. In this potential range, both 1F-EC and EC participates in the SEI-film formation. For the example of the 1F-EC/EC electrolyte system, the amount of active sites at the graphite surface, i.e. the graphite surface reactivity determines the mechanism of the SEI-film formation at the graphite electrode.

4. Conclusions

The surface properties of a highly crystalline graphite material has a significant influence on the electrolyte decomposition and passivation mechanism during the first electrochemical lithium insertion and thus on the SEI layer formation and composition. The SEI-film formation can be kinetically hindered at graphite surfaces with low surface reactivity. To predict the passivation behaviour of a graphite electrode material, the concept of the active surface area (ASA) is a suitable tool. The higher the fraction of the active surface area of the total graphite surface, i.e., the higher the amount of active surface sites at the graphite surface is, the higher is the graphite surface reactivity that can be expected. High values of ASA and d_{ASA} result in electrolyte decomposition and subsequent graphite surface passivation at potentials, which are more positive than the potential at which the electrochemical graphite exfoliation can be observed. Graphite electrode materials with high crystallinity, low superficial defect concentration, low amount of primatic surfaces, and low surface impurity concentration represent low ASA values and thus low surface reactivities towards electrolyte concentrations. To obtain a sufficient passivation of the graphite surface and an effective SEI-film formation the electrolyte composition needs to be adjusted with respect to the electrochemical reactivity towards the individual graphite surface.

Acknowledgements

Parts of this work were done under the auspices of the European research project CAMELiA (ENK6-CT2002-00636) supported by the European Community and the Swiss Federal Office of Education and Science. Dr. Olaf Böse, SOLVAY Fluor und Derivate (Hannover, Germany) is acknowledged for the preparation of the 1F-EC sample. The authors also thank the Swiss National Science Foundation for financial support.

References

[1] E. Peled, J. Electrochem. Soc. 126 (1979) 2047–2049.
[2] E. Peled, in: G.P. Gabano (Ed.), Lithium Batteries, Academic Press, New York, 1983, pp. 43–72.
[3] E. Peled, D. Golodnitsky, J. Penciner, in: J.O. Besenhard (Ed.), Handbook of Battery Materials, Wiley-VCH, New York, 1999, pp. 419–456.
[4] D. Aurbach, B. Markovsky, I. Weissmann, E. Levi, Y. Ein-Eli, Electrochim. Acta 45 (1999) 67–86.
[5] D. Aurbach, A. Zaban, Y. Ein-Eli, I. Weissmann, O. Chusid, B. Markovsky, M. Levi, E. Levi, A. Schechter, E. Granot, J. Power Sources 68 (1997) 91–98.
[6] J.O. Besenhard, M. Winter, J. Yang, W. Biberacher, J. Power Sources 54 (1995) 228–231.
[7] K.C. Möller, T. Hodal, W.K. Appel, M. Winter, J.O. Besenhard, J. Power Sources 97–98 (2001) 595–597.
[8] M. Morita, M. Ishikawa, Y. Matsuda, in: M. Wakaihara, O. Yamamoto (Eds.), Lithium Ion Batteries-Fundamentals and Performance, Wiley-VCH, Weinheim, 1998, pp. 156–180.
[9] F. Joho, B. Rykart, A. Blome, P. Novák, H. Wilhelm, M.E. Spahr, J. Power Sources 97–98 (2001) 78–82.
[10] F. Joho, P. Novák, M.E. Spahr, J. Electrochem. Soc. 149 (2002) A1020–A1024.
[11] M.E. Spahr, H. Wilhelm, F. Joho, P. Novák, ITE letters on batteries, New Technol. Med. 3 (3) (2001) 73–78.
[12] M.E. Spahr, H. Wilhelm, F. Joho, J.-C. Panitz, J. Wambach, P. Novák, N. Dupont-Pavlovsky, J. Electrochem. Soc. 149 (2002) A960–A966.
[13] M.E. Spahr, H. Wilhelm, T. Palladino, N. Dupont-Pavlovsky, D. Goers, F. Joho, P. Novák, J. Power Sources 119–121 (2003) 543–549.
[14] M.E. Spahr, T. Palladino, H. Wilhelm, A. Würsig, D. Goers, H. Buqa, M. Holzapfel, P. Novák, J. Electrochem. Soc. 151 (2004) A1383–A1395.
[15] A.N. Dey, B.P. Sullivan, J. Electrochem. Soc. 137 (1990) 222–224.
[16] R. Fong, U.V. Sacken, J.R. Dahn, J. Electrochem. Soc. 137 (1990) 2009–2013.
[17] J. Lahaye, Fuel 6 (1998) 543–547.
[18] C. Vix-Guterl, P. Ehrburger, in: P. Delhaes (Ed.), World of Carbon, Vol. 2, Taylor and Francis, London and New York, 2003, p. 188.
[19] H.P. Boehm, in: P. Delhaes (Ed.), World of Carbon, vol. 1, Taylor and Francis, Gordon and Breach, 2001, p. 141.
[20] N.R. Laine, F.J. Vastola, P.L. Walker Jr., J. Phys. Chem. 67 (1963) 2030–2034.
[21] P.J. Harat, F.J. Vastola, P.L. Walker Jr., Carbon 5 (1967) 363–371.
[22] W.P. Hoffman, F.J. Vastola, P.L. Walker, Carbon 22 (1984) 585–594.
[23] W.P. Hoffman, H.T. Phan, Carbon 33 (1995) 509–524.

[24] C. Vix-Guterl, I. Alix, P. Ehrburger, Acta Mater. 52 (6) (2004) 1639–1651.
[25] F. Béguin, F. Chevallier, C. Vix-Guterl, S. Saadallah, V. Bertagna, M. Letellier, J.N. Rouzaud, E. Frackowiak, J. Phys. Chem. Solids 65 (2004) 211–217.
[26] I.M.K. Ismail, Carbon 25 (1987) 653–662.
[27] P. Ehrburger, N. Pusset, P. Dziedzinl, Carbon 30 (1992) 1105–1109.
[28] C. Vix-Guterl, J. Dentzer, P. Ehrburger, K. Méténier, S. Bonnamy, F. Béguin, Carbon 39 (2001) 318–320.
[29] C. Vix-Guterl, G. Bekri, J. Dentzer, P. Ehrburger, J. Anal. Appl. Pyrolysis 67 (2003) 341–357.
[30] C. Vix-Guterl, M. Couzi, J. Dentzer, M. Trinquecoste, P. Delhaes, J. Phys. Chem., in press.
[31] D. Goers, H. Buqa, L. Hardwick, A. Würsig, P. Novák, Ionics 9 (2003) 258–265.
[32] K. Kinoshita, Electrochemical and Physicochemical Properties of Carbon, Wiley & Sons, New York, 1988.
[33] C.S. Wang, G.T. Wu und, W.Z. Li, J. Power Sources 76 (1998) 1–10.
[34] H. Huang, W. Liu, X. Huang, L. Chen, E.M. Kelder und, J. Schoonman, Solid State Ionics 110 (1998) 173–178.
[35] F. Tuinstra, J.L. Koenig, J. Chem. Phys. 53 (1970) 1126–1130.
[36] H. Wilhelm, M. Lelaurain, E. McRae, J. Appl. Phys. 84 (1998) 6552–6658.
[37] Y. Wang, D.C. Alsmeyer, R.L. McCreery, Chem. Mater. 2 (1990) 557–563.
[38] M.J. Matthews, M.A. Pimenta, G. Dresselhaus, M.S. Dresselhaus, M. Endo, Phys. Rev. B 59 (1999) R6585–R6588.
[39] A. Thomy, X. Duval, J. Regnier, Surf. Sci. Rep. 1 (1981) 1–38.
[40] T. Takaishi, Y. Sensui, Trans. Faraday Soc. 59 (1963) 2503–2514.
[41] P. Novák, W. Scheifele, F. Joho, O. Haas, J. Electrochem. Soc. 142 (1995) 2544–2550.
[42] R. Imhof, P. Novák, J. Electrochem. Soc. 145 (1998) 1081–1087.
[43] M. Winter, P. Novák, J. Electrochem. Soc. 145 (1998) L27–L30.
[44] M. Winter, R. Imhof, F. Joho, P. Novák, J. Power Sources 81–82 (2002) 818–823.